Twin relationship in between the variant-pair of η precipitates in the Al-Zn-Mg-Cu aluminium alloy

Tsai-Fu Chung[1], Yo-Lun Yang[2], Chien-Nan Hsiao[3], Wei-Chih Li[4], Jer-Ren Yang[1,]*

[1] Department of Materials Science and Engineering, National Taiwan University, Taipei, Taiwan.
[2] Department of Mechanical Engineering, Imperial College London, London SW7 2AZ, UK.
[3] Taiwan Instrument Research Institute, Hsinchu, Taiwan.
[4] E.A. Fischione Instruments, Inc., 9003 Corporate Circle, Export, PA 15632, U.S.A.

Abstract. For Al-Zn-Mg-Cu aluminium alloys, 15 types of η precipitates would possess the symmetrically variants distributed on the closed planes of the Al matrix, parallel to the $(0001)\eta$, $(2\bar{1}\bar{1}0)\eta$, or $(10\bar{1}0)\eta$ interfaces of precipitates. The η_2 precipitates, possessing the crystallographic orientation of $(1\bar{1}\bar{1})_{Al}$ // $(0001)\eta_2$ and $[110]_{Al}$ // $[10\bar{1}0]\eta_2$, would exhibit four equivalent variants, i.e., $\eta_2^{(1)}$ to $\eta_2^{(4)}$, on the $(1\bar{1}\bar{1})_{Al}$ habit planes. In the present work, along the zone axis of $[110]_{Al}$ // $[10\bar{1}0]\eta$, the edge-on configurations showing the twin-like atomic arrays would occur as the growth/coalescence of two η_2 variants grown on $(1\bar{1}\bar{1})_{Al}$ and $(1\bar{1}1)_{Al}$ planes, respectively. The twin relationship can be revealed in term of the crystallographic relationship at 70.5° with respect to their habit planes. Alternatively, on the $(\bar{1}\bar{1}0)_{Al}$ image, it also indicates the nearly-twinning configuration in between the variant-pair of η_2.

1. Introduction

The Al-Zn-Mg-Cu aluminium alloys, exhibiting the high strength mechanical property, are well known to be applied in the automotive and aerospace applications. The precipitation hardening of the AA7050 aluminium alloys [1-9] begins from the fully or nearly coherent GP zones (GPI and GPII zones), and subsequently transforms into the semi-coherent η' precipitates (4 variants), and then the incoherent η precipitates (15 types, η_1-η_{14}, and η_4'). In the recent work, The nucleation and transformation mechanisms of GPII zones → η' precipitates and η' precipitates → η_2 precipitates have been recognized as the separated and in-situ nucleations, which are conducted by the in-situ frames of micrographs and the serial Fast-Fourier-Transform (FFT) diffractograms of high-resolution transmission electron microscopy (HRTEM), respectively [1].

According to the in-situ transformation mechanism of η' precipitates → η_2 precipitates and their identical crystallographic orientations with respect to the Al matrix : $[10\bar{1}0]\eta'$ // $[110]_{Al}$ and $(0001)\eta'$ // $(1\bar{1}\bar{1})_{Al}$ of η' precipitates, and $[10\bar{1}0]\eta_2$ // $[110]_{Al}$ and $(0001)\eta_2$ // $(1\bar{1}\bar{1})_{Al}$ of η_2 precipitates [1, 10], it would be observed four equivalent variants of η_2 (i.e., $\eta_2^{(1)}$ precipitates to $\eta_2^{(4)}$ precipitates), grown on the respective $(1\bar{1}\bar{1})_{Al}$ habit planes, as portrayed in Fig. 1. Afterwards, employed by Cs-corrected high-angle annular-dark-field (HAADF) scanning-transmission electron microscopy (STEM) [2], the edge-on configurations of four η_2 along the zone axis of $[10\bar{1}0]\eta_2$ // $[110]_{Al}$ are characterized as the sandwiched stacking arrangements, in which the regular variations of Zn and Mg layers subsequently stacks on the $(0001)\eta_2$ // $(1\bar{1}\bar{1})_{Al}$ habit planes.

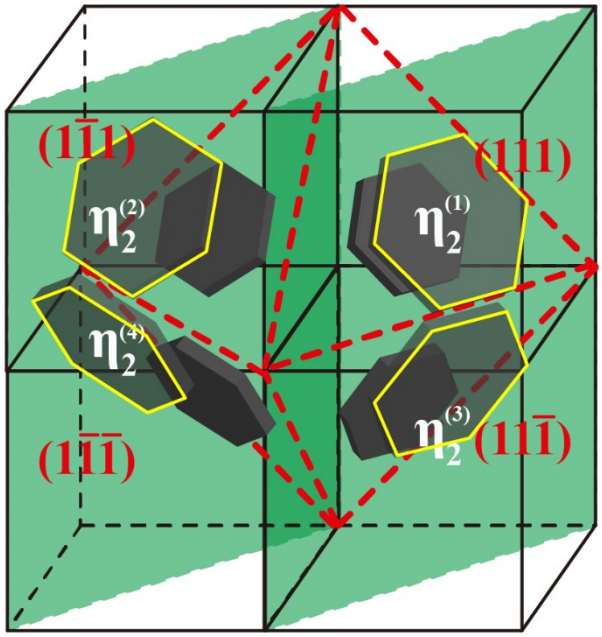

Fig. 1 The schematic diagram of four variants of η_2 precipitates (i.e., $\eta_2^{(1)}$ to $\eta_2^{(4)}$) grow on $\{111\}_{Al}$ habit planes. As the precipitate growing, the coarsened η_2 are indicated by yellow frames.

It has been reported that the distributions in between the orientational variants of precipitates would be easily misunderstood from the 2-dimensional projections of the 3-dimensional phenomena [11, 12]. For example, in the Al-Cu-(Li) aluminium alloys [11], the impingements are inevitably caused by the overlap of two edge-on variants of θ'-Al_2Cu precipitates, in which their habit planes are parallel to the $(100)_{Al}$ and $(010)_{Al}$ planes of the Al matrix, respectively. On the other hand, in the recent work employed by HAADF-STEM [12], the joint of two edge-on variants of θ' incisively revealed the distributed

* Corresponding author: author@e-mail.org

arrangements, implying that the possibility of the interaction between the orientational variants of precipitates. However, so far there is no direct experimental to support the crystallographic relationship such as twinning relationship in between two variants of θ'. Tacitly, in the Al-Zn-Mg-Cu aluminium alloys, whether the crystallographic distribution of the 15 typed η precipitates (i.e., η_1-η_{14}, and η_4') and their corresponding variants [1, 2] would also exist the crystallographic relationship in between themselves has yet to be elucidated.

In the present work, employed by Cs-corrected HAADF STEM, we especially focused on the crystallographic relationships of η_2 and their variant pairs in Al-Zn-Mg-Cu aluminium alloys. Along the zone axis of $[110]_{Al}$, the detailed atomic configurations of η_2 has been revealed. Additionally, the crystallographic relationship in between variant-pair of η_2 has been confirmed under the observation of $[110]_{Al}$ and $[\bar{1}\bar{1}0]_{Al}$ zone axes

2. Materials and methods

The AA7050 aluminium alloy (Al-6.25Zn-2.14Mg-2.23Cu, wt.%) was used in this study. After solution treatment (at 475 °C for 1 h with water quenching), the samples were treated with a three-step ageing treatment: (1) ageing at 120 °C for 8 h, (2) ageing at 165 °C for 1 h, and subsequently (3) ageing at 174 °C for 8 h with an applied constant tensile stress of 162.5 MPa at the same time (named as creep-age forming samples, CAF samples). The TEM specimens were prepared by cutting discs from the selected samples for observing the pancaked structures and thinning the discs to the thickness of 65 - 70 μm before they were twin-jet electropolished in a mixture of 0.33 HNO_3 and 0.67 CH_3OH at -20 °C with a working voltage of 10-11 V, as shown in Fig. 2.

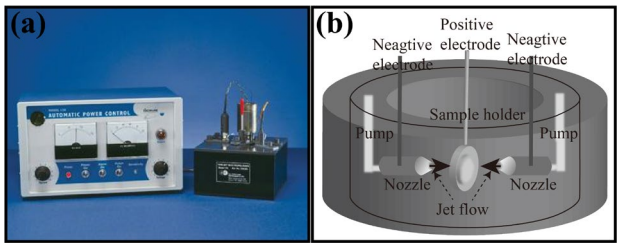

Fig. 2 (a) The twin-jet electropolishing instrument (E.A. Fischione Instrument), and (b) the schematic inward of twin-jet system.

The oxidation layers of specimens was removed and the corresponding thickness was reduced with an M1040 NanoMill system (E.A. Fischione Instrument), as shown in Fig. 3a and then the hydrocarbon contamination was cleaned by an M1070 Nanoclean plasma (E.A. Fischione Instrument), as shown in Fig. 3b. Afterwards, the TEM specimens were observed with an FEI Titan Chemi-STEM equipped with a spherical aberration corrector (Cs-corrector), under the 135 nm camera length and with a collecting angle range of ~8.24 mrad (inner angle) to ~143.6 mrad (outer angle) of a HAADF detector.

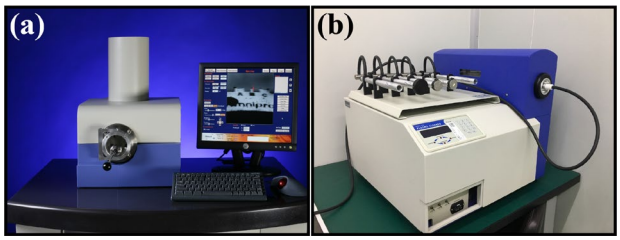

Fig. 3 (a) M1040 NanoMill system, and (b) M1070 Nanoclean plasma system.

3. Results & Discussion

Fig. 4a shows the edge-on configuration of η_2 grown on the $(\bar{1}11)_{Al}$ habit plane, and its atomic arrangement along the $[110]_{Al}$ zone axis. The alternative brightness-darkness Z-contrast can be explained by the stimulated atomic image based on first principle calculation, as shown in Fig. 4b. The interweaving Zn and Mg atomic-layers are consistent with the brighter Z-contrast representing Zn-rich layers and the lower Z-contrast, the Mg/Zn layers. This result is similar to the sandwiched stacking of η_2, repored in our previpus work [2]. Moreover, in Fig. 4c, the FFT diffractogram, this paeticle can be recognized as $\eta_2^{(4)}$ crystal exhibiting the crystallographic relationship with respect to the Al matrix: $[10\bar{1}0]\eta_2^{(4)}$ // $[110]_{Al}$ and $(0001)\eta_2^{(4)}$ // $(\bar{1}11)_{Al}$.

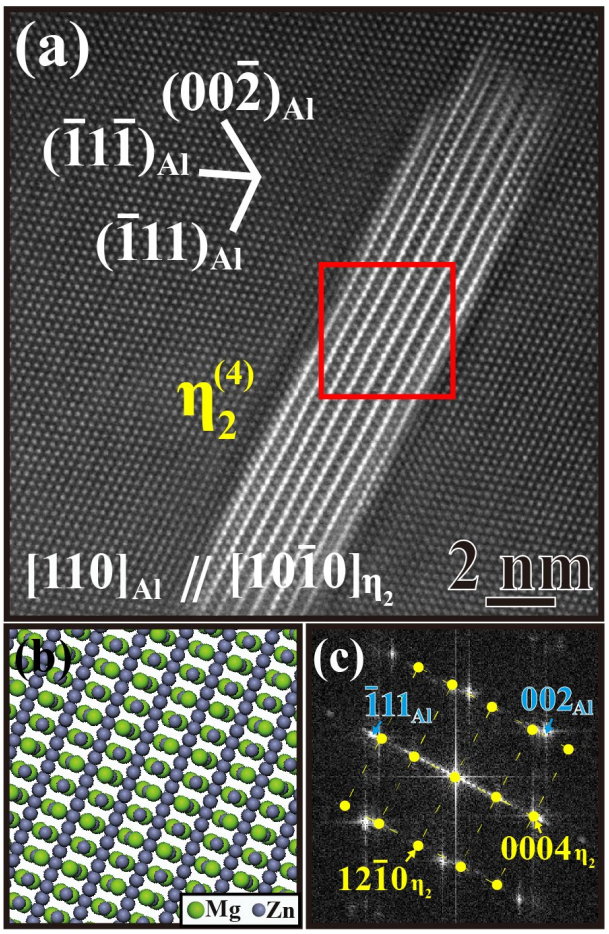

Fig. 4 (a) The STEM image showing the edge-on configuration of $\eta_2^{(4)}$ along the $[110]_{Al}$ zone axis [13]. (b) Stimulated atomic-stacking. (c) FFT diffractogram.

Fig. 5a shows that two edge-on configurations of two variants of η_2 (i.e., $\eta_2^{(2)}$ and $\eta_2^{(4)}$) exhibiting the sandwiched stacking structure on the $(0001)\eta_2$ // $(\bar{1}1\bar{1})_{Al}$ and $(0001)\eta_4$ // $(\bar{1}11)_{Al}$ habit planes, respectively. Their different size can be ascribed to the difference in the growth rate. Particularly, the joint area, i.e., the interweaved interface, between $\eta_2^{(2)}$ and $\eta_2^{(4)}$ possesses a twinning relationship with an angle of 109.5° between the $(00\bar{2})_{Al}$ plane, as marked by the red lines in Fig. 5a. Here, it can be ascribed to two phenomena. First, the collision of two variants of η_2 occurred as they grow, the so-called hard impingement [12, 14]. Secondly, these two η_2 would develop at the same interface of the nucleation stage. we temporarily call the intrinsic boundary.

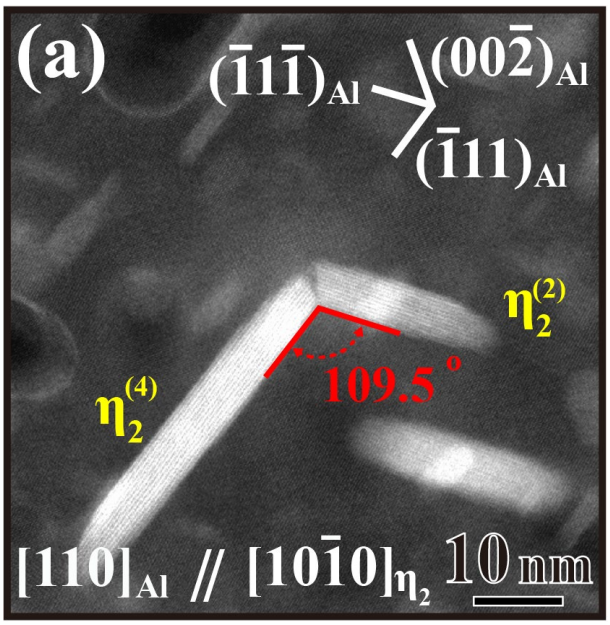

Fig. 5 (a) HAADF STEM image showing the two edge-on configurations of η_2 precipitate (i.e., $\eta_2^{(2)}$ and $\eta_2^{(4)}$) grown on the $(0001)\eta_2$ // $(\bar{1}1\bar{1})_{Al}$ and $(0001)\eta_4$ // $(\bar{1}11)_{Al}$ habit planes, respectively under the $[110]_{Al}$ // $[10\bar{1}0]\eta_2$ zone axis [13].

For the detailed investigation on the atomic arrangement and microstructural evolution in between two variants of η_2 (i.e., $\eta_2^{(2)}$ and $\eta_2^{(4)}$), the area with the nearly darkness Z-contrast (as marked by the red arrow in Fig 5b) can be recognized as segregation of vacancies or Mg solute atoms. This given area was supposedly ascribed to the early stage of nucleation. As the growth of these two variants of η_2, vacancies and Mg atoms are gradually annihilated by the substitutions of Zn and Cu solute atoms. Finally, the mismatched interface would turn into the well-matched interface (as marked by the solid dot of the red arrow in Fig. 5b). Whether the intrinsic boundary would be observed in 15 typed η under the observation of $[110]_{Al}$, $[001]_{Al}$ and $[11\bar{2}]_{Al}$ zone axes has yet to be reported.

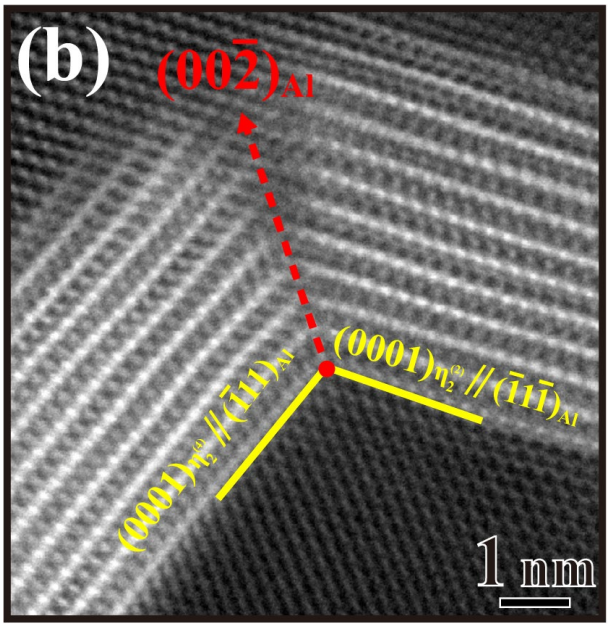

Fig. 5 (b) A enlarged image of (a) revealing the twin relationship of an angle of 109.5° between the $(00\bar{2})_{Al}$ plane with respect to the $(0001)\eta_2^{(2)}$ // $(\bar{1}\,1\,\bar{1})_{Al}$ and $(0001)\eta_2^{(4)}$ // $(\bar{1}11)_{Al}$ habit planes [13].

Another case crystallographic relationship of different variants of η_2 is shown in Fig. 6a. Specially, the joint area (Fig. 6) is totally different from the end of two variants, as shown in Fig. 5. Along the zone axis of $[110]_{Al}$, the edge-on configurations of $\eta_2^{(2)}$ and $\eta_2^{(4)}$, grown on the $(0001)\eta_2$ // $(\bar{1}1\bar{1})_{Al}$ and $(0001)\eta_4$ // $(\bar{1}11)_{Al}$ habit planes, respectively, reveal the twinning relationship with an angle of 109.5° or 70.5° with respect to two different twinning planes in between these two variants.

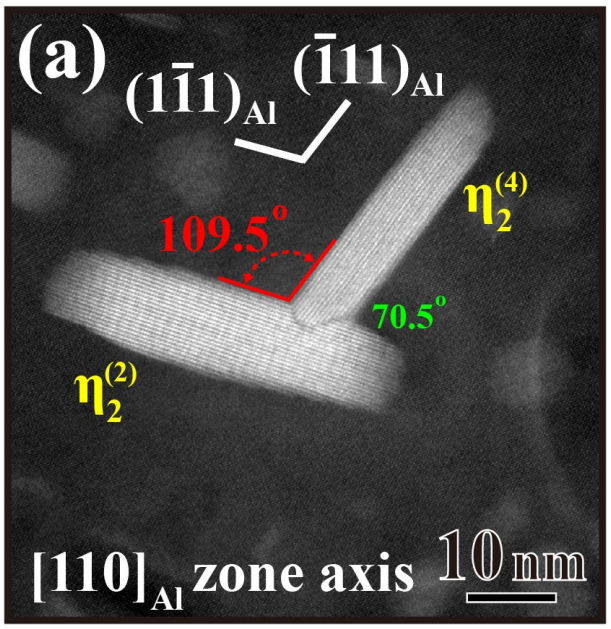

Fig. 6 (a) HAADF STEM image showing the twinning relationship with an angle of 109.5° or 70.5° twinning relationship with an angle of 109.5° respect to two edge-on configurations of $\eta_2^{(2)}$ and $\eta_2^{(4)}$ along the zone axis of $[110]_{Al}$.

Similarly, the detailed study on the atomic configurations in between $\eta_2^{(2)}$ and $\eta_2^{(4)}$ are illustrated in Fig. 6b. It has been found that the twin relationships of two angles of 109.5° and 70.5° between the $(1\bar{1}3)_{Al}$ and $(\bar{3}31)_{Al}$ planes of the Al matrix, respectively. The coherent twin boundaries would be caused by the nucleation and growth, instead of the effect of the hard impingement. It could be suggested that the nucleation site would be the partial segregation of Zn/Cu nearby the interfaces between the η_2 precipitate and the Al matrix with the abnormally strong bright Z-contrast, reported in the previous work [2]. In the present case, the nuclei would be located on the interfaces of $\eta_2^{(2)}$ and would follow the twinning relationship as the growth of precipitates.

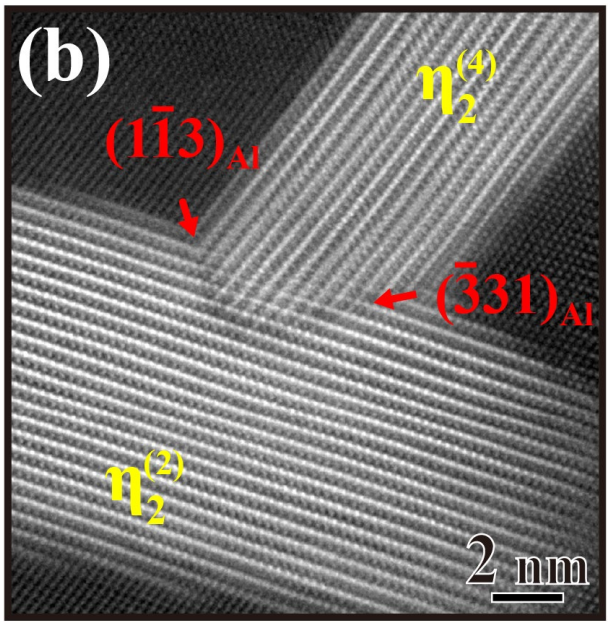

Fig. 6 (b) A enlarged image of (a) revealing the twin relationships of two angles of 109.5° and 70.5° between the $(1\bar{1}3)_{Al}$ and $(\bar{3}31)_{Al}$ planes with respect to $\eta_2^{(2)}$ and $\eta_2^{(4)}$ precipitates.

Furthermore, in Fig. 7, the edge-on configurations of $\eta_2^{(2)}$ and $\eta_2^{(4)}$ are specifically observed along the zone axis of $[\bar{1}\bar{1}0]_{Al}$ with respect to the resulted HAADF STEM image of Fig. 6. At the joint or intersected position, the crystallographic relationship in twinning would exist. However, one coherent twinning boundary, as indicated by the red arrow in Fig. 7, can be found. It can be suggested that the segregations of Zn/Cu to be the nucleation site of $\eta_2^{(4)}$ would locate on the part of the $\eta_2^{(2)}$/Al interfaces.

Conclusively, according to the orientation relationships of 15 typed η precipitates (η_1-η_{14}, and η_4') and the corresponding variants, their crystallographic relationships are related to be twinning. In the present work, along the zone axes of $[110]_{Al}$ and $[\bar{1}\bar{1}0]_{Al}$, it can be fount the twinning boundaries in between the edge-on configurations of $\eta_2^{(2)}$ and $\eta_2^{(4)}$.

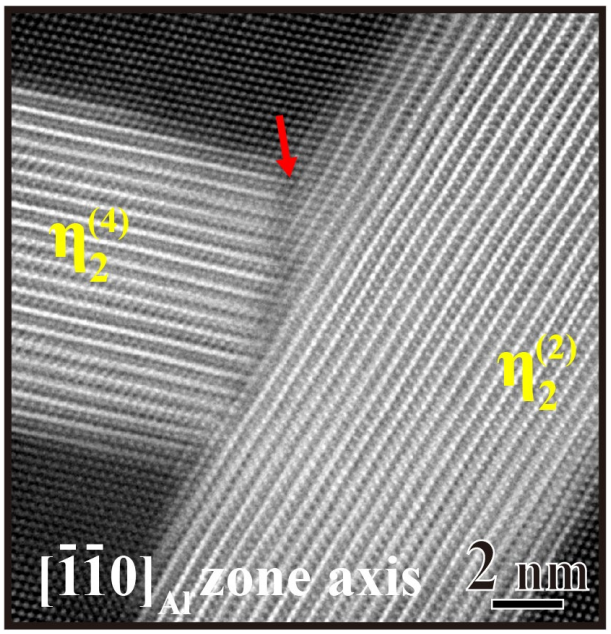

Fig. 7 HAADF STEM image along the zone axis of $[\bar{1}\bar{1}0]_{Al}$ with respect to that of Fig. 6 revealing the atomic configuration of the joint area in between $\eta_2^{(2)}$ and $\eta_2^{(4)}$.

4. Acknowledgements

This work was carried out with the financial support from Foundation for the Advancement of Outstanding Scholarship and Ministry of Science and Technology (Taiwan) under Contract MOST108-2622-E-002-016-CC2. The authors are grateful to Taiwan Instrument Research Institute and Materials Analysis Technology Inc. (MA-tek) for technical advice.

5. Reference

[1] T.-F. Chung, Y.-L. Yang, B.-M. Huang, Z. Shi, J. Lin, T. Ohmura, J.-R. Yang, Acta Mater. **149** (2018).
[2] T.-F. Chung, Y.-L. Yang, M. Shiojiri, C.-N. Hsiao, W.-C. Li, C.-S. Tsao, Z. Shi, J. Lin, J.-R. Yang, Acta Mater. **174** (2019).
[3] A. Deschamps, A. Bigot, F. Livet, P. Auger, Y. Brechet, D. Blavette, Philos. Mag. A **81** (2001).
[4] A. Deschamps, F. Bley, F. Livet, D. Fabregue, L. David, Philosophical Magazine **83** (2003).
[5] L. Couturier, A. Deschamps, F. De Geuser, F. Fazeli, W.J. Poole, Scripta Mater. **136** (2017).
[6] C.R. Hutchinson, F. de Geuser, Y. Chen, A. Deschamps, Acta Mater. **74** (2014).
[7] A. Bendo, K. Matsuda, A. Lervik, T. Tsuru, K. Nishimura, N. Nunomura, R. Holmestad, C.D. Marioara, K. Shimizu, H. Toda, Mater. Charact. (2019).
[8] H. Degischer, W. Lacom, A. Zahra, C. Zahra, Z. Metallk. **71** (1980).
[9] J. Gjønnes, C.J. Simensen, Acta. Metall. Mater. **18** (1970).
[10] S. Ringer, K. Hono, Mater. Charact. **44** (2000).
[11] J. da Costa Teixeira, D.G. Cram, L. Bourgeois, T.J. Bastow, A.J. Hill, C.R. Hutchinson, Acta Mater. **56** (2008).
[12] T.-F. Chung, Y.-L. Yang, C.-N. Hsiao, W.-C. Li, B.-M. Huang, C.-S. Tsao, Z. Shi, J. Lin, P.E. Fischione, T.

Ohmura, J.-R. Yang, International Journal of Lightweight Materials and Manufacture **1** (2018).
[13] T.-F. Chung, Y.-L. Yang, M. Shiojiri, C.-N. Hsiao, W.-C. Li, J.-R. Yang, Procedia Manufacturing **37** (2019).
[14] B. Decreus, A. Deschamps, F. De Geuser, P. Donnadieu, C. Sigli, M. Weyland, Acta Mater. **61** (2013).